ACS APPLIED MATERIALS & INTERFACES

Research Article

www.acsami.org

Metal–Organic Coordination-Enabled Layer-by-Layer Self-Assembly to Prepare Hybrid Microcapsules for Efficient Enzyme Immobilization

Xiaoli Wang, Zhongyi Jiang, Jiafu Shi, Yanpeng Liang, Chunhong Zhang, and Hong Wu*

Key Laboratory for Green Chemical Technology of Ministry of Education, School of Chemical Engineering and Technology, Tianjin University, Tianjin, P. R. China

ABSTRACT: A novel layer-by-layer self-assembly approach enabled by metal–organic coordination was developed to prepare polymer-inorganic hybrid microcapsules. Alginate was first activated via N-ethyl-N′-(3-dimethylaminopropyl) carbodiimide (EDC) and N-hydroxy succinimide (NHS) coupling chemistry, and subsequently reacted with dopamine. Afterward, the dopamine modified alginate (Alg-DA) and titanium(IV) bis(ammonium lactato) dihydroxide (Ti(IV)) were alternatively deposited onto $CaCO_3$ templates. The coordination reaction between the catechol groups of Alg-DA and the Ti(IV) allowed the alternative assembly to form a series of multilayers. After removing the templates, the alginate-titanium hybrid microcapsules were obtained. The high mechanical stability of hybrid microcapsules was demonstrated by osmotic pressure experiment. Furthermore, the hybrid microcapsules displayed superior thermal stability due to Ti(IV) coordination. Catalase (CAT) was used as model enzyme, either encapsulated inside or covalently attached on the surface of the resultant microcapsules. No CAT leakage from the microcapsules was detected after incubation for 48 h. The encapsulated CAT, with a loading capacity of 450–500 mg g^{-1} microcapsules, exhibited desirable long-term storage stability, whereas the covalently attached CAT, with a loading capacity of 100–150 mg g^{-1} microcapsules, showed desirable operational stability.

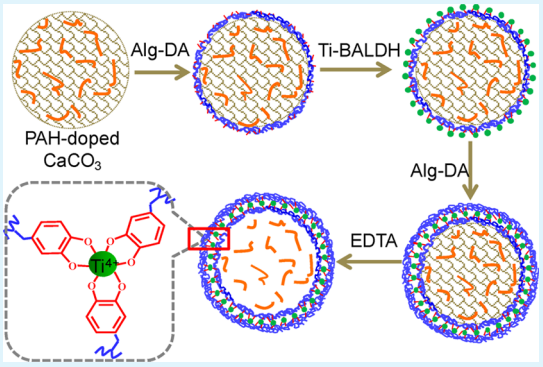

KEYWORDS: *layer-by-layer self-assembly, titanium(IV)-catecholate complex, hybrid microcapsule, alginate, enzyme immobilization*

INTRODUCTION

Polymer–inorganic hybrid materials aroused a lot of recent interest from the viewpoints of both scientific research and technological applications. Particularly, polymer–inorganic hybrid microcapsules have been widely used in biomacromolecules encapsulation for catalysis,[1] drug or gene delivery,[2] cell technology,[3] etc.

At present, hybrid capsules are usually prepared by LbL assembly processes involving two different approaches. One is liquid-phase deposition of charged inorganic particles and oppositely charged polymers.[4−6] The other involves the infiltration of polyelectrolyte multilayers on colloid spheres with sol–gel precursors, confining the sol–gel reaction to the polyelectrolyte shell.[7,8] However, the accompanying problems, such as the preparation of inorganic nanoparticles prior to electrostatic adsorption[9] and the reliance of aggressive organic solvent to dissolve reactive alkoxide precursors[10] make the fabrication process tedious and environmentally unfriendly.

In our previous studies, hybrid microcapsules have been prepared via a synergy between biomimetic mineralization and layer-by-layer self-assembly strategy.[11,12] The protamine layer induced the hydrolysis and condensation of titania precursor, to form the titania layer in situ. Additionally, by introducing an additional bioadhesion layer, improved strength and surface reactivity of the hybrid microcapsules were gained.[13] Here we describe a strategy of incorporating metal–organic coordination into LbL assembly to prepare hybrid microcapsules with high strength and thermal stability.

Metal–organic coordination is ubiquitous in nature, particularly in load-bearing exoskeletal biomaterials[14,15] and has fascinated many researchers due to the delicate structures and superior properties.[16−20] Metal–organic coordination endows not only a peculiar combination of hardness (100–150 MPa) and extensibility (>70% strain),[21,22] but also a covalent-like stability.[23] It would be highly desirable to import these attributes into LbL self-assembly process to acquire the hybrid microcapsules in a facile and controllable way. LbL assembly based on metal–organic coordination has a long research history,[24−26] but titanium(IV)-ligand coordination for layer-by-layer deposition has never been studied.

In this study, a mussel adhesive protein-mimetic polyanion, the dopamine-modified alginate (Alg-DA), was synthesized by the conjugation of dopamine onto alginate with the assistance of the EDC/NHS coupling chemistry. Then, alternate deposition of Alg-DA and titanium(IV) bis(ammonium lactato) dihydroxide on $CaCO_3$ templates until a desired layer number was acquired. After removal of templates, the polymer-inorganic hybrid microcapsules were obtained. The size and

Received: March 30, 2012
Accepted: June 24, 2012
Published: June 24, 2012

   dx.doi.org/10.1021/am300559j | ACS Appl. Mater. Interfaces 2012, 4, 3476–3483

shell thickness of the hybrid microcapsules could be easily controlled by the size of $CaCO_3$ templates and the number of deposited layers. The catechol groups of Alg-DA can react with amine and thiol,[27,28] which thereof endowed the microcapsules with tunable surface reactivity. The microcapsules were then utilized to anchor model enzyme, catalase (CAT), either through physical encapsulation or covalent linkage.

MATERIALS AND METHODS

Materials. Catalase (hydrogen peroxide oxidoreductase; 2000–5000 units mg^{-1} protein EC.1.11.1.6) from bovine liver, titanium(IV) bis(ammonium lactato) dihydroxide (Ti-BALDH, 50 wt % aqueous solution), poly(allylamine hydrochloride) (PAH, MW ca.70 000), poly(sodium. 4-styrenesulfonate) (PSS, MW ca. 70 000), poly(ethyleneimine) (PEI, MW = 750 000, 50 wt % aqueous solution) and fluorescein isothiocyanate (FITC) were purchased from Sigma–Aldrich Chemical Co.. Dopamine hydrochloride was purchased from Yuancheng Technology Development Co. Ltd. (Wuhan, China). Polyacrylonitrile (PAN) membrane with a molecular weight cutoff of 80,000 was gained from Shanghai MegaVision Membrane Engineering & Technology Co. Ltd. (Shanghai, China).1-Ethyl-3-[3-dimethylaminopropyl] carbodiimide hydrochloride (EDC) and N-hydroxysuccinimide (NHS) were purchased from Shanghai Medpep Co. Ltd. Tris(hydroxymethyl)amiomethane (Tris), ethylenediaminetetra acetic acid (EDTA), hydrogen peroxide (H_2O_2, 30 wt %), sodium alginate, sodium dihydrogen phosphate dehydrate ($NaH_2PO_4{\cdot}2H_2O$) and sodium phosphate dibasic dodecahydrate ($Na_2HPO_4{\cdot}12H_2O$) were purchased from Tianjin Guangfu Fine Chemical Research Institute (Tianjin, China). The water used in all experiments was treated by the Millipore Milli-Q purification system. Fluorescent-labeled enzymes were prepared using overnight incubation at room temperature of their mixtures with FITC (0.05 M phosphate buffer, pH 8.0, protein concentration 1 mg mL^{-1}, [dye]/[enzyme] = 5) followed by exhaustive dialysis (MW cutoff 14 000) against phosphate buffer (0.05 M pH 7.0) for 72 h and deionized water for 24 h.

Synthesis of Dopamine-Modified Alginate (Alg-DA). 1 g of alginate (5.05 mmol in terms of repeating unit) was dissolved in 100 mL of PBS buffer solution (50 mM, pH 5.5). Equal molar amounts of NHS and EDC (5.05 mmol) were added in the above solution. The reaction mixture was stirred at room temperature for 45 min to fully activate the carboxylic groups on alginate molecules. Then, prescribed amount of dopamine was added into the above mixture and then stirred for 12 h at room temperature under N_2 protection. The product was precipitated with alcohol for three times followed by lyophilization. Dopamine modified alginate with different graft ratio were obtained by varying the molar ratio of alginate to dopamine (1:0.5, 1:1.0, 1:2.0) and denoted as Alg-$DA_{0.5}$, Alg-$DA_{1.0}$, and Alg-$DA_{2.0}$, respectively.

Fabrication of Ti(IV)-Catecholate Hybrid Microcapsules. Four milligrams of PAH was dissolved in 4 mL of 0.33 M $CaCl_2$ solution, and an equal volume of 0.33 M Na_2CO_3 solution was then rapidly poured and stirred for 30 s at room temperature. After settling for 20 min without stirring, the PAH-doped $CaCO_3$ microparticles were centrifuged and washed with water to remove residual PAH and salts. The PAH-doped $CaCO_3$ microparticles were then alternately suspended in Alg-DA solution (7 mL, 1.5 mg mL^{-1}) for 20 min and Ti-BALDH solution (7 mL, 40 mM) for 5 min. LbL microcapsules with the bilayer architecture of $(Alg\text{-}DA/Ti)_n$ were prepared, where n was the number of bilayers. One bilayer was constructed by depositing an Alg-DA layer, followed by a Ti layer. The capsules were rinsed with water three times after each layer deposition. The Ti(IV)-catecholate hybrid microcapsules were obtained by removing the $CaCO_3$ cores in an EDTA solution (50 mM, pH 7.0).

Encapsulation of CAT inside Hybrid Microcapsules. Six milligrans of CAT was dissolved in 1 mL of Tris-HCl buffer solution (50 mM, pH 7.0). The enzyme solution was added into the 4 mL of 0.33 M $CaCl_2$ solution. The CAT-encapsulated hybrid microcapsules were prepared following the same procedure as described above.

Covalent Attachment of CAT onto the Hybrid Microcapsules. The as-prepared hybrid microcapsules with Alg-DA as outermost layer were lyophilized prior to utilization. Then, 3 mg of the microcapsules were suspended in 8 mL 0.2 mg mL^{-1} of CAT solution in Tris-HCl buffer solution (50 mM, pH 7.0) for 8 h at room temperature to allow covalent attachment of the enzyme molecules onto the microcapsule surface.

Characterizations. SEM images of the microcapsules were recorded by using an environmental scanning electron microscope (ESEM, Philips XL30) and a field-emission scanning electron microscope (FESEM, Nanosem 430). Elemental analysis of the microcapsules was accomplished by energy dispersive spectroscope (EDS) attached to ESEM. TEM observation of the microcapsules was performed on a JEM-100CX II instrument. Elemental compositions of the Alg-DA polymers were performed by Elementar Vatio EL CUBE. The zeta-potentials of microparticle surface were measured in water using a Brookhaven zeta-potential analyzer. Three parallel measurements were conducted for each sample, and the absolute errors were not exceeding ±4 mV. A contact angle goniometer (JC2000C Contact Angle Meter, Powereach Co., Shanghai, China) was used to measure the contact angle of multilayers. Fluorescence microscope images of microcapsules were taken using an Olympus BX51 microscope with a 100× oil immersion objective lens (Olympus, Tokyo, Japan). UV–vis spectra of the Alg-DA polymer solutions were monitored at wavelengths from 191 to 400 nm at a scan rate of 800 nm min^{-1} by UV–vis (Hitachi U-3010) spectrophotometer. The enzyme concentration was measured by UV–vis (Hitachi U-3010) spectrophotometer. Thermogravimetric analysis (TGA) was performed on a Perkin-Elmer Pyris analyzer.

Loading Capacity. The amount of immobilized CAT was determined by measuring the final concentrations of CAT with washing solution using Coomassie Brilliant Blue reagent, following the Bradford's method.[29]

The loading capacity was determined according to eq 1

$$M\left(\frac{\text{mg of enzyme}}{\text{g of support}}\right) = \left(\frac{m - C_1V_1}{W}\right) \quad (1)$$

where M (mg g^{-1}) represented the loading capacity; m (mg) was the amount of CAT introduced into the immobilization medium; C_1 (mg mL^{-1}) and V_1 (mL) were the enzyme concentration and volume of the washing solution, respectively; W (g) was the weight of the microcapsules.

Leakage Ratio and Activity Assay. The leakage ratio of CAT was defined as the ratio of cumulative leakage amount of CAT to initial amount of encapsulated CAT. To examine the leakage of CAT from hybrid microcapsules, CAT-containing microcapsules were added into 7 mL buffer solution of Tris-HCl (50 mM, pH 7.0), and incubated for 48 h at room temperature under mild shaking. The mixture was then centrifuged, and the content of CAT in the supernate was determined by the Bradford's method using Coomassie Brilliant Blue reagent.

The activity of immobilized enzyme or free enzyme was determined spectrophotometrically by measuring the decrease in the absorbance of hydrogen peroxide at 240 nm due to the enzymatic decomposition.[30] Briefly, the immobilized enzyme (or free enzyme) was added to 19.58 mM H_2O_2 in Tris-HCl (50 mM, pH 7.0) at 20 °C under stirring. After 5 min, the decrease in absorbance at 240 nm was recorded and the enzyme activity was calculated according to eq 2

$$2H_2O_2 \xrightarrow{\text{CAT}} 2H_2O + O_2 \quad (2)$$

one unit of CAT will decompose 1 μmol of H_2O_2 per min at pH 7.0 and 20 °C. The relative enzyme activity was calculated by comparing the activity of immobilized enzyme with that of equal amount of free enzyme.

Kinetic Parameters (K_m and V_{max}). K_m and V_{max} for the free and immobilized enzymes were determined using the Michaelis–Menten model, given by eq 3

$$\frac{1}{V} = \frac{K_m}{V_{max}} \times \frac{1}{[S]} + \frac{1}{V_{max}} \quad (3)$$

where V (mM min^{-1}) was the initial reaction rate, $[S]$ (mM) was the initial substrate concentration, V_{max} (mM min^{-1}) was the maximum reaction rate attained at infinite initial substrate concentration and K_m (mM) was the Michaelis–Menten contant.

To determine the K_m and V_{max}, the activity assay was applied to different hydrogen peroxide concentrations from 3 mM to 35 mM. Enzyme activity was determined at 30 °C in Tris-HCl (50 mM, pH 7.0). Kinetic parameters for both the free and the immobilized CAT were calculated accordingly.

Stabilities. The immobilized CAT was collected after each reaction batch, and washed with Tris-HCl (50 mM, pH 7.0) to remove any residual substrate and then added to the next reaction cycle. The reusability stability of immobilized CAT was explored by measuring the enzyme activity in each successive reaction cycle and expressed by recycling efficiency.

The effects of pH and temperature on the activity for free and immobilized CAT were determined by measuring the residual activity of enzyme at 30 °C in Tris-HCl (50 mM, pH 7.0) after being exposed to different temperatures (25–70 °C) and pH (4.0–9.0) in 50 mM Tris-HCl for 3 h.

Free and immobilized CAT were stored in Tris-HCl (50 mM, pH 7.0) at 4 °C for a certain period of time. The storage stability was compared in terms of storage efficiency defined as the ratio of the activity of free or immobilized enzyme after storage to their initial activities.

RESULTS AND DISCUSSION

Synthesis and Characterization of Dopamine-Modified Alginate. Dopamine-modified alginate (Alg-DA) was synthesized using EDC/NHS chemistry as illustrated in Figure.1. EDC reacted with the carboxylic groups on alginate to form an O-acylisourea intermediate which was very unstable and susceptible to hydrolysis. The addition of NHS could stabilize the O-acylisourea intermediate by converting it to an amine-reactive NHS ester (succinimidyl ester). Then, the amine-reactive ester reacted with dopamine to form the Alg-DA polymers. During the reaction, N_2 was used as protection gas in order to avoid the self-polymerization of dopamine. The graft ratio of dopamine was controlled by varying the molar ratio of dopamine to alginate. The as-synthesized Alg-DA polymers were gray fibrous solids and became colorless when dissolved in water.

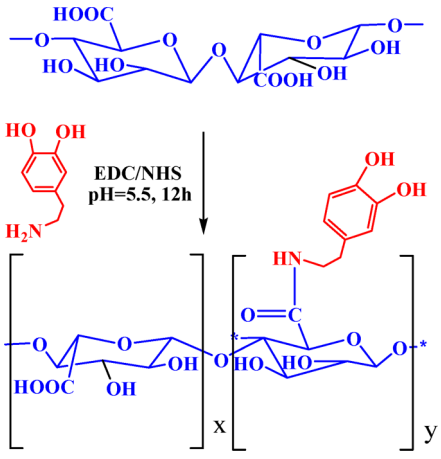

Figure 1. Schematic of representation of the synthesis process of dopamine modified alginate (Alg-DA).

UV–vis spectra of the Alg-DA polymer solutions were monitored, and shown in Figure.2a. After grafting with dopamine, a new peak appeared at 280 nm and strengthened as the dopamine content increased. The new peak was ascribed to the stretching of the catechol groups from dopamine.[31,32] This result validated the successful synthesis of alginate conjugated with different content of dopamine.

To determine the graft ratio of the Alg-DA polymers, the C, N, and H elements were detected by combustion analysis. The N/C ratios were listed in Table 1. The N element was from the amine groups of dopamine ($C_8H_{11}NO_2$), and the C element was from both alginate (monomer: $C_6H_7NaO_3$) and dopamine. Therefore, the graft ratio was determined according to N/C ratio, given by eq 4

$$\text{graft ratio} = \frac{y}{x+y} = \frac{6N/C}{1 - 8N/C} \quad (4)$$

where y represented the number of modified alginate monomers, x represented the number of unmodified alginate monomers, 6 and 8 were the numbers of carbon atoms in alginate monomers and dopamine, respectively. As shown in Table 1, the higher the content of dopamine, the higher the graft ratio formed and thus the more binding sites for Ti(IV) ions. The graft ratio could reach 42% when the molar ratio of dopamine to alginate was 2.0.

Upon addition of Ti-BALDH to Alg-DA polymers solution, an immediate color change from transparent to yellow (see Figure 2b) was observed, indicating coordination of catechol to the Ti^{4+} ion. Moreover, the color of the mixture deepened with the increasing of the graft ratio of Alg-DA polymers. The higher graft ratio the Alg-DA polymers, the more coordination complexes generated, hence a deeper color of the mixed solution. Wilker et al.[33] mentioned that the vivid yellow species was coordination complexes with three catecholate ligands bound to a Ti^{4+} ion. Actually, the charge of Ti^{4+} resulted in high affinity toward ligands with negatively charged and hard oxygen donor groups. This high affinity resulted in only partial formation of Ti(IV) bis-catecholate prior to facile generation of Ti(IV) tris-catecholate.[33]

Fabrication and Characterization of Hybrid Microcapsules. A viable approach to construct the hybrid microcapsules metal-catecholate coordination-based has been demonstrated. Iron(III)-catecholate complexes are widely distributed in biological systems. However, the solubility of Fe^{3+} is very low at alkaline and neutral pH (at pH 7, only 1×10^{-18} M aqueous Fe^{3+} is present in solution,[34] a slight deviation of pH values to the alkaline side leads to the precipitation of iron hydroxide). Ti is similar to Fe in the capability to form high valent ions. The strong Lewis acidity of Ti^{4+} ions, in turn, leads to greater affinities toward the highly electronegative catecholate.[33] Therefore, titanium(IV) is chosen to construct hybrid microcapsules instead of iron(III). Simultaneously, the catechol ligand has the optimal geometry for binding to Ti ions; resulting in ring coordination complexes of catecholate type (binuclear bidentate binding–bridging) thus generates the six-coordinated octahedral geometry of Ti ions.

The Ti(IV)-catecholate hybrid microcapsules were obtained by deposition from aqueous solution onto PAH-doped $CaCO_3$ particles as shown in Figure.3. The PAH-doped $CaCO_3$ were prepared via coprecipitation and ready as sacrificial templates for the subsequent preparation of microcapsules. The obtained microparticles were alternately suspended in Alg-DA and Ti-

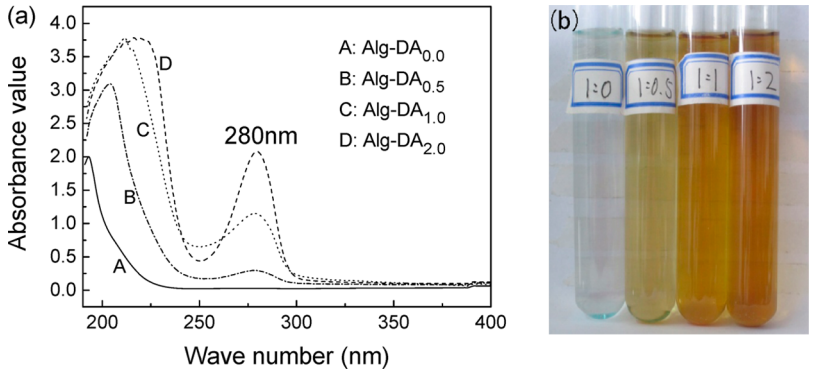

Figure 2. (a) UV−vis spectra of Alg-DA$_x$ aqueous solutions; (b) solution images of Ti-BALDH and Alg-DA$_x$ (x = 0.0,0.5, 1.0, 2.0).

Table 1. Graft Ratio of Dopamine-Modified Alginate (Alg-DA)

	molar ratio alginate to dopamine		
	1:0.5	1:1.0	1:2.0
N/C*100	3.84	3.93	4.49
graft ratio (%)	33.3	34.4	42.0

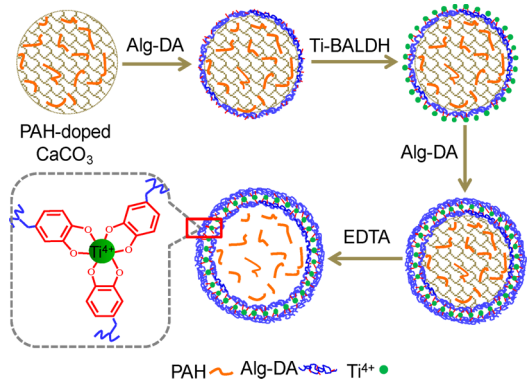

Figure 3. Schematic representation of the fabrication process of hybrid microcapsules.

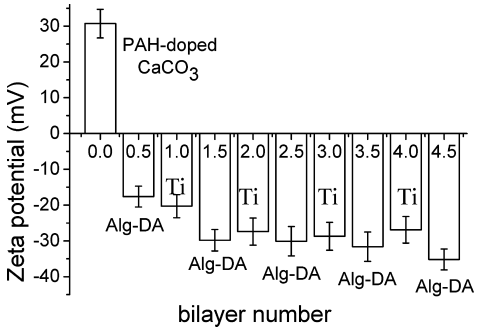

Figure 4. Zeta-potentials as a function of layer number during the LBL deposition of Alg-DA$_{2.0}$ and Ti(IV) on PAH-doped $CaCO_3$ microparticles in water (25 °C, pH7.0).

BALDH solution to form (Alg-DA/Ti)$_n$ layers. After that, an additional Alg-DA layer was deposited, yielding the (Alg-DA/Ti)$_{n+0.5}$ microparticles with Alg-DA as the outermost layer. The final hybrid microcapsules were obtained after removing the $CaCO_3$ templates.

To confirm deposition of Alg-DA or Ti(IV) onto the particles, zeta-potential measurements on PAH-doped $CaCO_3$ particles prior to and after deposition of different layers were performed in aqueous solution as shown in Figure.4. The bare PAH-doped $CaCO_3$ particles were positively charged (30.7

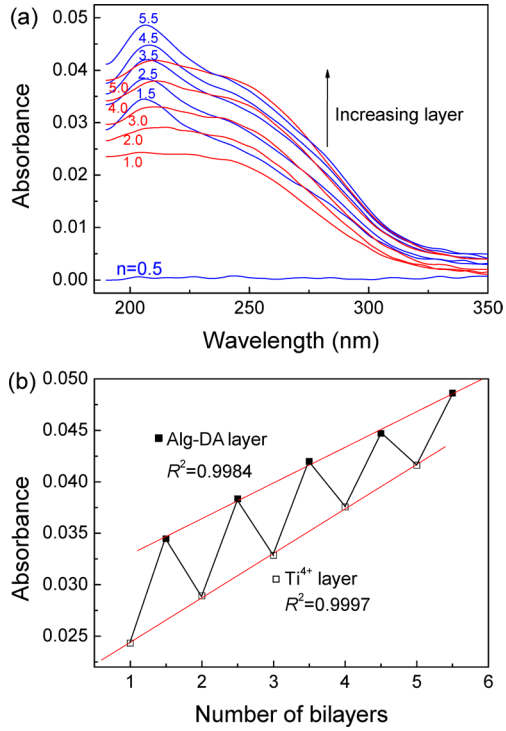

Figure 5. (a) UV−vis spectra of (Alg-DA$_{2.0}$/Ti)$_n$ multilayer; (b) optical absorption at λ_{max} = 206.5 nm for Alg-DA layers and Ti^{4+} layers.

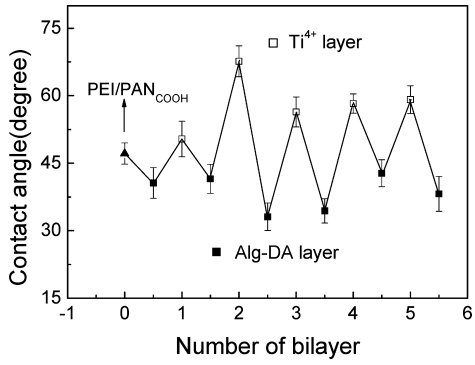

Figure 6. Variations in water contact angles during the construction of the (Alg-DA$_{2.0}$/Ti)$_n$ multilayer on the hydrolytic PAN film. Layer 0 indicates the precoated PEI film.

dx.doi.org/10.1021/am300559j | ACS Appl. Mater. Interfaces 2012, 4, 3476−3483

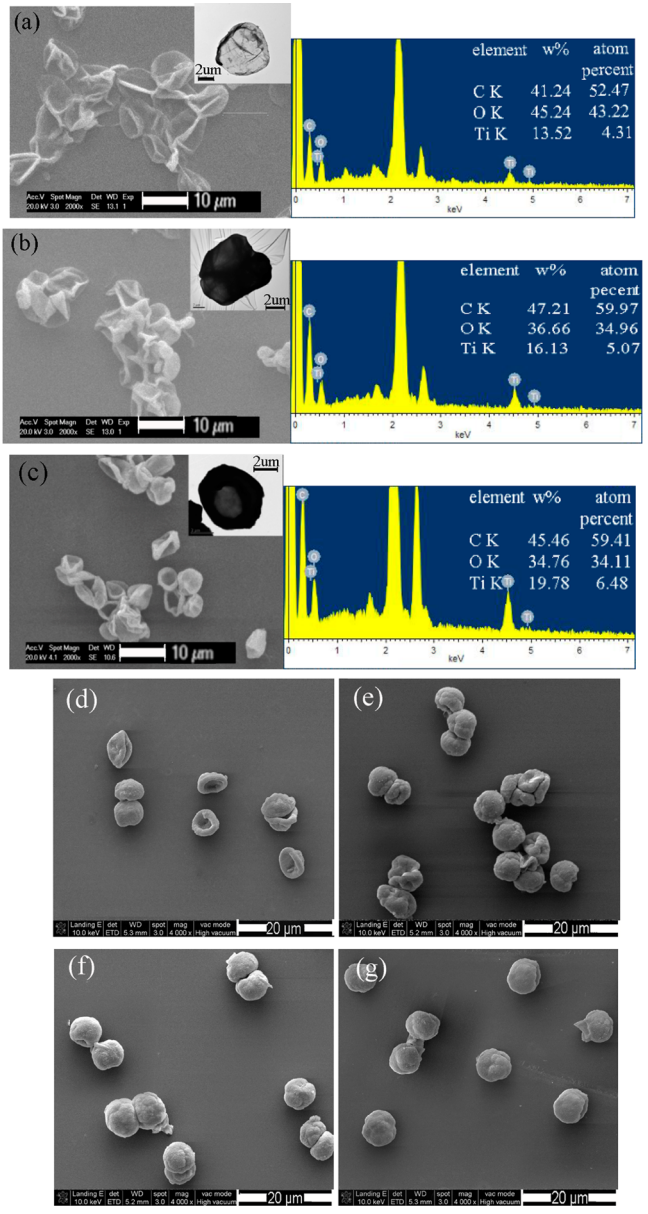

Figure 7. SEM, TEM (inset) and EDS images of $(Alg\text{-}DA_x/Ti)_{1.5}$: (a) x = 0.5, (b) x = 1.0, (c) x = 2.0; FESEM images of $(Alg\text{-}DA_{2.0}/Ti)_n$ microcapsules, (d) n = 1.5, (e) n = 2.5, (f) n = 3.5, (g) n = 4.5.

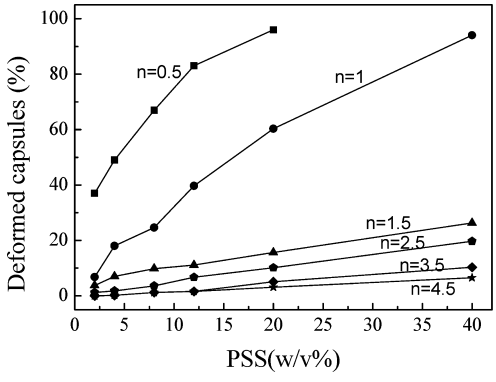

Figure 8. Percentage of deformed $(Alg\text{-}DA_{2.0}/Ti)_n$ microcapsules as a function of the PSS concentration.

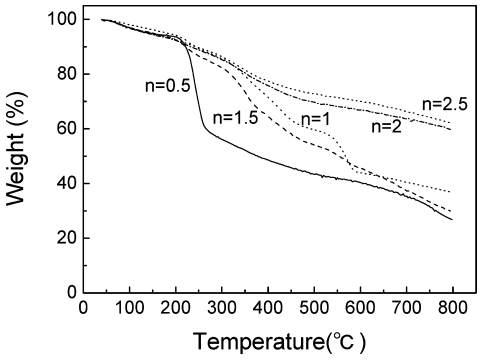

Figure 9. TGA curves of $(Alg\text{-}DA_{2.0}/Ti)_n$ microcapsules.

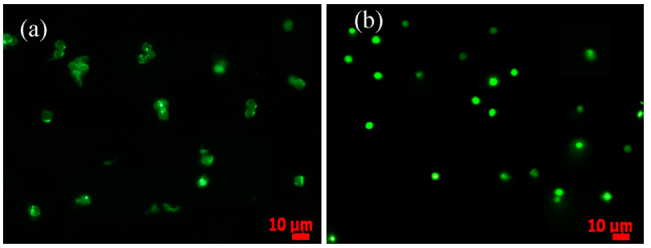

Figure 10. Fluorescence microscope images of (a) FITC-labeled CAT-encapsulated microcapsules, (b) FITC-labeled CAT-attached microcapsules.

Table 2. Kinetic Parameters of Free, Encapsulated and Covalently Attached CAT

	K_m (mM)	V_{max} (mM min^{-1})
free	41.13	27.94
covalently attached	42.32	25.24
encapsulated	67.52	19.12

mV) ensuring the deposition of the negatively charged Alg-$DA_{1.0}$, whereas the zeta-potential of $CaCO_3$ particles was −28 mV in the absence of PAH.[35] The doping of PAH endowed the surface of $CaCO_3$ particles with positive charge. After deposition of the negatively charged Alg-$DA_{1.0}$, surface charge of the 0.5-bilayer particles inverted to slightly negative (−11.8 mV), indicating that the deposition of Alg-$DA_{1.0}$ layer was a result of electrostatic interactions and hydrogen bonds. Subsequently, suspension of the particles in Ti-BALDH solution changed the surface charge of $(Alg\text{-}DA_{1.0}/Ti)_1$ from −11.8 to −20.7 mV, inferring that the Ti^{4+} coordinated with Alg-$DA_{1.0}$ at the particles surface. Further suspension of the particles in Alg-$DA_{1.0}$, surface charge of the $(Alg\text{-}DA_{1.0}/Ti)_{1.5}$ changed to −31.6 mV, indicating that the Alg-$DA_{1.0}$ reacted with Ti^{4+} again. These particles were negatively charged indicated that LbL assembly did not depend on electrostatic interaction. It was worth mentioning that the surface charge of 1.5-bilayer particles was much higher than that of 0.5-bilayer particles, although their outmost layers were the same (Alg-$DA_{1.0}$). The carboxyl groups were more acidic than the catechol groups, suggesting its higher affinity toward the positive PAH-doped $CaCO_3$ particles. As for the 0.5-bilayer particles, the carboxyl main chains of Alg-$DA_{1.0}$ oriented to the PAH-doped $CaCO_3$ particles, and the catechol side chains oriented outward, rendering the particles low surface charge. As for the 1.5-bilayer particles, the catechol side chains of the outer Alg-$DA_{1.0}$ layer oriented inward in order to bind Ti(IV) ions. Therefore, the

dx.doi.org/10.1021/am300559j | ACS Appl. Mater. Interfaces 2012, 4, 3476−3483

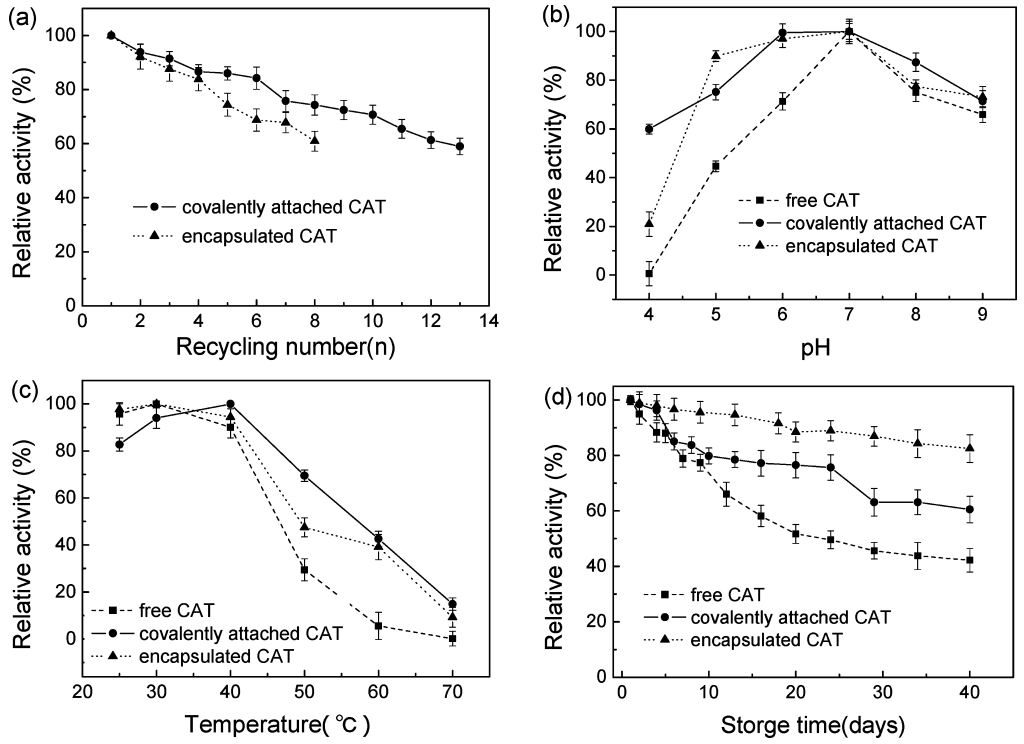

Figure 11. (a) Relative activity (%) represented the ratio of residual activity to initial activity of each sample; (b) Activity at pH 7.0 was normalized to 100%; (c) relative activity (%) represented the ratio of residual activity to highest activity of each sample; (d) activity of the first day was normalized to 100%.

main chains-containing the more negative carboxyl groups endowed the 1.5-bilayer particles higher surface charge. The phenomenon was attributed to the coordination geometry that metal ion could orient the organic ligands in space.[36]

To further investigate the layer build-up procedure, multilayer film based on LbL assembly and metal−organic coordination was prepared. A quartz plate (size 25 mm ×12 mm ×1 mm) was cleaned with the RCA cleaning solution (5:1:1 H_2O:H_2O_2 (30%):NH_3 (25%)) at 60 °C for 30 min, rinsed with deionized water and dried under a stream of nitrogen gas. The clean slides were first immersed in PEI solution (5 mg mL^{-1}) for 30 min to form the self-assembled monolayer terminated with $-NH_2$ functional groups at the exposed surface. The precoated PEI slides were then alternately immersed in Alg-$DA_{2.0}$ solution (1.5 mg mL^{-1}, 20 mL) and Ti-BALDH (40 mM, 20 mL) solution for 5 min. The substrates were washed with water and dried with a nitrogen stream after each immersion. By repeating the above procedure, PEI−(Alg-$DA_{2.0}$/Ti)$_n$, multilayer films were prepared. The assembly procedure was characterized by UV−vis spectra. Figure.5a showed the UV−vis spectra of the (Alg-$DA_{2.0}$/Ti)$_n$ films (n = 0.5−5.5). The absorbance at 206.5 nm vs the number of bilayer was plotted in Figure.5b. The growth of the film exhibited a good linear correlation with correlation coefficients of R^2 = 0.9997 and R^2 = 0.9984 for assembly of Ti layer and Alg-DA layer, respectively, suggesting the formation of a microstructurally regular multilayer structure. The metal−organic coordination interactions were responsible for the LbL deposition between the Ti ions and the Alg-DA polymer.

Wettability of the multilayer film after each assembly was investigated by measuring the water contact angles as shown in Figure 6. Five measurements at different spots were carried out for each specimen and the accuracy of the measurement was ± 2°. Before the construction of the (Alg-$DA_{2.0}$/Ti)$_n$ multilayer, PAN films (size 25 mm ×60 mm) were first hydrolyzed with 1 M NaOH solution at 60 °C for 2 h. The contact angles alternated between Alg-DA-terminated and Ti^{4+}-terminated layers, indicating regular formation of a multilayer. The contact angle of the Alg-DA-terminated layer was lower than that of Ti^{4+}-terminated layer due to the higher hydrophilicity of the Alg-DA than the coordination complexes.

Figure 7a-c showed SEM and TEM images of (Alg-DA_x/Ti)$_{1.5}$ with x = 0.5, 1.0, and 2.0. SEM images showed the hybrid microcapsules with a diameter of ca. 5 μm. The microcapsules were flattened and collapsed but not ruptured during drying due to interior water evaporation. TEM images further confirmed the hollow and unbroken structure. The graft ratio of dopamine modified alginate had a significant effect on the capsule shell thickness. Figure 7d−g showed the FESEM images of (Alg-$DA_{2.0}$/Ti)$_n$ with n = 1.5, 2.5, 3.5, 4.5. After drying, microcapsules with n = 1.5, 2.5 exhibited the morphology of folds and creases but not ruptured, suggesting the hollow structure. Microcapsules with n = 3.5, 4.5 kept a regular spherical shape, indicating that the shell of hybrid microcapsules had strong mechanical strength. The coordination of titanium ion between layers rendered the hybrid microcapsules with appropriate structural flexibility and mechanical strength.

Energy dispersive spectroscopy (EDS) analysis of the (Alg-DA_x/Ti)$_{1.5}$ with x = 0.5, 1.0, and 2.0 indicated the presence of C, O, and Ti elements (see Figure 7a−c). The peak intensity of Ti element increased with gradually increasing graft ratio of Alg-DA polymers. Because a higher graft ratio of Alg-DA polymer would afford more catechol moieties to combine more Ti(IV) ions, the Ti/C atom ratio of Alg-$DA_{0.5}$ microcapsules (0.082) was less than that of Alg-$DA_{2.0}$ microcapsules (0.109).

dx.doi.org/10.1021/am300559j | ACS Appl. Mater. Interfaces 2012, 4, 3476−3483

The mechanical stability of microcapsules was assessed by the method of penetrated pressure in different concentration of PSS aqueous solution. About 200 microcapsules were inspected at each PSS concentration. Microcapsules kept their initial shape at low PSS concentrations, and microcapsules broke or shrunk at high PSS concentrations. The large PSS molecules (MW ca.70 000) could not pass through the microcapsule shell. The shrinking/buckling of hollow capsules was caused by excess osmotic pressure of the outer PSS solution. The percentage of deformed microcapsule was an indication of the mechanical stability of microcapsules. As shown in Figure 8, 90% and 60% of $(Alg\text{-}DA_{2.0})$ and $(Alg\text{-}DA_{2.0}/Ti)_1$ microcapsules were deformed in 20 w/v% PSS solution. In 40 w/v% PSS solution, $(Alg\text{-}DA_{2.0})$ microcapsules were totally broken, whereas only ~30% and ~20% of $(Alg\text{-}DA_{2.0}/Ti)_{1.5}$ and $(Alg\text{-}DA_{2.0}/Ti)_{2.5}$ microcapsules were shrunk but not broken. The mechanical stability of the microcapsules was significantly improved by Ti(IV)-catecholate coordination between layers. Moreover, the mechanical stability of microcapsules increased with the increase of layers. Besides, the mechanical stability of hybrid microcapsules was higher than that of capsules prepared with only polyelectrolytes.

To further testify the coordination effect of Ti(IV) ions, TGA curves(see Figure 9) of microcapsules coated with different layers were compared. In the present investigation, heating rates were suitably controlled at 10 °C min^{-1} under nitrogen atmosphere with flow rate 20 mL min^{-1} and the weight loss is measured from the ambient temperature up to 800 °C. Because organic material cannot be completely combusted under N_2 atmosphere, the residue mass of $Alg\text{-}DA_{2.0}$ microcapsules without Ti was 26.79wt.-% and the residue of $(Alg\text{-}DA_{2.0}/Ti)_n$ ($n > 0.5$) was composed of both carbon (ash) and TiO_2. TGA showed that the residue weights of $(Alg\text{-}DA_{2.0}/Ti)_2$ and $(Alg\text{-}DA_{2.0}/Ti)_{2.5}$ were 60.14 wt % and 62.15 wt % much higher than 26.79 wt % of $(Alg\text{-}DA_{2.0})$ microcapsules. According to the thermal decomposition of $(Alg\text{-}DA_{2.0})$ microcapsules, the drastic weight loss temperature at 221.5 °C corresponded to the stripping of the aromatic ring of the side chain. The TGA curve for $(Alg\text{-}DA_{2.0}/Ti)_1$ microcapsules did not show the drastic weight loss at 221.5 °C while showed a slight weight loss peak at 560 °C. Besides, the thermal degradation for $(Alg\text{-}DA_{2.0}/Ti)_{1.5}$, $(Alg\text{-}DA_{2.0}/Ti)_2$, and $(Alg\text{-}DA_{2.0}/Ti)_{2.5}$ microcapsules did not show any drastic weight loss. The above results confirmed that the thermal properties were reinforced by the coordination effect of Ti(IV) ions. Moreover, the thermal stability of microcapsules increased with the increase of layer number. Especially, thermal stability was improved greatly after assembling a titanium layer.

Activities and Stabilities of Immobilized Enzymes. To demonstrate the feasibility of LbL assembled hybrid microcapsules as enzyme immobilization supports, CAT-encapsulated and CAT-attached microcapsules were individually prepared. The CAT was encapsulated inside microcapsules via coprecipitation of $CaCO_3$. The outmost layer of the as-prepared hybrid microcapsules was Alg-DA polymer on which the catechol groups provided a convenient route to immobilize enzyme through amine-catechol adduct formation. Consequently, CAT was covalently attached onto the microcapsules via coupling between catechol and enzyme amine.[27,37] The activity and stability of the CAT encapsulated in or covalently attached to the $(Alg\text{-}DA_{1.0}/Ti)_{1.5}$ microcapsules were investigated in the subsequent experiments.

Images a and b in Figure 10 showed the fluorescence microscope images of FITC-labeled CAT-encapsulated and FITC-labeled CAT-attached microcapsules. The fluorescence signals revealed the successful encapsulation of CAT inside microcapsules (see Figure 10a) and covalent attachment of CAT onto the surface of the microcapsules (see Figure 10b).

The loading capacity of CAT encapsulated inside microcapsules achieved 450−500 mg g^{-1} dry microcapsules, and that of the covalently attached CAT onto the microcapsules achieved 100−150 mg g^{-1} dry microcapsules.

The relative enzyme activity of encapsulated and covalently attached CAT retained 34 and 65% of free enzyme activity, respectively. The decrease of enzyme activity could be a result of some denaturation and increased diffusion resistance of substrate to immobilized enzyme. The relative activity of covalently attached CAT was higher than that of encapsulated CAT because of the reduced inner diffusion limitation. Besides, the high loading inside the hybrid microcapsules might also prevent the use of all CAT present. Furthermore, no leakage of CAT encapsulated inside microcapsules was detected, validating the Ti(IV) ions coordination effectively avoided the leakage of enzyme.

Kinetic parameters were measured for free, encapsulated and covalently attached CAT at 25 °C, pH 7.0. The Michaelis constant (K_m) and the maximum reaction rate (V_{max}) were calculated from Lineweaver−Burk plots (the data was not shown here). The values of K_m and V_{max} were listed in Table 2. The lower value of K_m indicated the higher affinity of enzyme toward substrate.[39] The comparable K_m values for free and covalently attached CAT (41.13 mM vs 42.32 mM) indicated almost the identical affinity toward the H_2O_2 molecules. It can be derived that the three-dimensional conformation and active sites of the enzyme were well-preserved. In contrast to free CAT, the low K_m values indicated that the affinity of encapsulated CAT toward substrate was slightly influenced because of additional diffusion resistance occurring in the encapsulation method. The V_{max} value reflected the intrinsic characteristic of the immobilized enzyme but may be affected by diffusion constrains.[42] The covalently attached CAT molecules were located on the outer surface of supports, therefore, achieved almost the identical V_{max} values compared to that of free CAT. In contrast, the V_{max} value for encapsulated CAT was lower than that of free CAT, indicated that the inner diffusion lowered the accessibility of substrates to the active sites on enzyme molecules.

Figure 11a. showed the stability that was very important for immobilized enzymes in view of their potential industrial applications. The recycling stability was investigated by conducting successive batches of H_2O_2 decomposition. The encapsulated and covalently attached CAT retained about 60% of its initial activity after 8 and 13 batches, respectively. The decrease in activity was due to the mass loss of microcapsules during the centrifugation.

The stabilities of free, encapsulated, and covalently attached CAT against extreme pHs (4−9), heat (25−70 °C) and storage time were probed. The encapsulated and covalently attached CAT both showed higher activities over a wider pH range than free CAT counterpart (see Figure 11b). As for thermal stability, free CAT lost about 70% of its activity whereas the encapsulated and covalently attached CAT separately lost about 50 and 30% of their activities after 3 h preincubation time at 50 °C (see Figure 11c). The results suggested the enhanced thermal stability after immobilization. At last, the storage

stabilities for both the encapsulated and covalently attached CAT were significantly higher than that for free CAT (see Figure 11d). And this result indicated that both immobilization methods could effectively maintain enzyme activity. Specifically, the encapsulated CAT retained 82% of its initial activity after storing for 40 days, indicating that the microcapsules provided an appropriate environment for enzyme molecules. Moreover, the stabilities of CAT immobilized in the hybrid microcapsules were higher than the microcapsules prepared with only polyelectrolytes, which usually swell severely and even partly or totally dissolve responding to a change of pH, salt concentration, and temperature.

CONCLUSIONS

A novel approach to polymer-inorganic hybrid microcapsules was developed by incorporating metal−organic coordination into LbL assembly. The dopamine-modified alginate and titanium(IV) bis(ammonium lactato) dihydroxide were alternatively deposited on $CaCO_3$ templates. The Ti(IV)-catecholate coordination enabled the robust and controllable self-assembly. Accordingly, the shell thickness and the consequent physical/chemical properties of the hybrid microcapsules could be tuned by the number of deposited layers. The hybrid microcapsules have been demonstrated as the efficient and stable carriers for enzyme immobilization, the encapsulated enzyme acquired high catalytic activity while the covalently attached enzyme exhibited significantly improved recycling stability. Because of the ubiquity of metal−organic coordination and the wide applicability of LbL self-assembly, this approach may be useful for preparing a variety of polymer−inorganic hybrid materials with tailored structures and different properties.

AUTHOR INFORMATION

Corresponding Author

*Fax: +86 022 2789 0882. Tel: +86 22 2350 0086. E-mail: wuhong2000@gmail.com.

Notes

The authors declare no competing financial interest.

ACKNOWLEDGMENTS

The authors thank the financial support from the National Basic Research Program of China (2009CB724705), National Science Fund for Distinguished Young Scholars (21125627), the National Science Foundation of China (20976127, 21076145), Program for New Century Excellent Talents in University (NCET-10-0623), the Program of Introducing Talents of Discipline to Universities (B06006), and the Natural Science Foundation of Tianjin (09JCYBJC06700).

REFERENCES

(1) Shi, J.; Zhang, L.; Jiang, Z. *ACS Appl. Mater. Interfaces* **2011**, *3*, 881−889.
(2) Gokmen, M. T.; De Geest, B. G.; Hennink, W. E.; Du Prez, F. E. *ACS Appl. Mater. Interfaces* **2009**, *1*, 1196−1202.
(3) Fakhrullin, R. F.; Minullina, R. T. *Langmuir* **2009**, *25*, 6617−6621.
(4) Strohm, H.; Sgraja, M.; Bertling, J.; Löbmann, P. *J. Mater. Sci.* **2003**, *38*, 1605−1609.
(5) Qiao, R.; Zhang, X. L.; Qiu, R.; Kim, J. C.; Kang, Y. S. *Chem. Mater.* **2007**, *19*, 6485−6491.
(6) Caruso, F.; Caruso, R. A.; Möhwald, H. *Science* **1998**, *282*, 1111−1114.
(7) Laugel, N.; Hemmerlé, J.; Porcel, C.; Voegel, J.-C.; Schaaf, P.; Ball, V. *Langmuir* **2007**, *23*, 3706−3711.
(8) Shchukin, D. G.; Caruso, R. A. *Chem. Mater.* **2004**, *16*, 2287−2292.
(9) Niu, P.; Hao, J. *Langmuir* **2011**, *27*, 13590−13597.
(10) Yu, A.; Lu, G.; Drennan, J.; Gentle, I. R. *Adv. Funct. Mater.* **2007**, *17*, 2600−2605.
(11) Jiang, Y.; Yang, D.; Zhang, L.; Sun, Q.; Sun, X.; Li, J.; Jiang, Z. *Adv. Funct. Mater.* **2009**, *19*, 150−156.
(12) Li, J.; Jiang, Z.; Wu, H.; Zhang, L.; Long, L.; Jiang, Y. *Soft Matter* **2010**, *6*, 542−550.
(13) Zhang, L.; Shi, J.; Jiang, Z.; Jiang, Y.; Meng, R.; Zhu, Y.; Liang, Y.; Zheng, Y. *ACS Appl. Mater. Interfaces* **2011**, *3*, 597−605.
(14) Broomell, C. C.; Khan, R. K.; Moses, D. N.; Miserez, A.; Pontin, M. G.; Stucky, G. D.; Zok, F. W.; Waite, J. H. *J. R. Soc. Interface* **2007**, *4*, 19−31.
(15) Lichtenegger, H. C.; Birkedal, H.; Waite, J. H. Heavy metals in the jaws of invertebrates. In *Biomineralization: From Nature to Application*; Metal Ions in Life Sciences; Sigel, A., Sigel, H., Sigel, R. K. O., Eds.; John Wiley & Sons: Chichester, U.K., 2008; Vol. *4*, p 295.
(16) Griffith, C. S.; Reyes, M. D. L.; Scales, N.; Hanna, J. V.; Luca, V. *ACS Appl. Mater. Interfaces* **2010**, *2*, 3436−3446.
(17) Harrington, M.; Masic, A.; Holten-Andersen, N.; Waite, J.; Fratzl, P. *Science* **2010**, *328*, 216−220.
(18) Zeng, H.; Hwang, D. S.; Israelachvili, J. N.; Waite, J. H. *Proc. Natl. Acad. Sci. U.S.A. Early Ed.* **2010**, *107*, 12850−12854.
(19) Suzuki, M.; Waraksa, C. C.; Mallouk, T. E.; Nakayama, H.; Hanabusa, K. *J. Phys. Chem. B* **2002**, *106*, 4227−4231.
(20) Mazur, M.; Krysiński, P.; Blanchard, G. J. *Langmuir* **2005**, *21*, 8802−8808.
(21) Whittell, G. R.; Manners, I. *Adv. Mater.* **2007**, *19*, 3439−3468.
(22) Holten-Andersen, N.; Fantner, G. E.; Hohlbauch, S.; Waite, J. H.; Zok, F. W. *Nat. Mater.* **2007**, *6*, 669−672.
(23) Holten-Andersen, N.; Harrington, M. J.; Birkedal, H.; Lee, B. P.; Messersmith, P. B.; Lee, K. Y. C.; Waite, J. H. *Proc. Natl. Acad. Sci. U.S.A.* **2011**, *108*, 2651−2655.
(24) Wanunu, M.; Vaskevich, A.; Cohen, S. R.; Cohen, H.; Arad-Yellin, R.; Shanzer, A.; Rubinstein, I. *J. Am. Chem. Soc.* **2005**, *127*, 17877−17887.
(25) Hatzor, A.; Moav, T.; Cohen, H.; Matlis, S.; Libman, J.; Vaskevich, A.; Shanzer, A.; Rubinstein, I. *J. Am. Chem. Soc.* **1998**, *120*, 13469−13477.
(26) Maier, A.; Rabindranath, A. R.; Tieke, B. *Chem. Mater.* **2009**, *21*, 3668−3676.
(27) Zhu, L. P.; Jiang, J. H.; Zhu, B. K.; Xu, Y. Y. *Colloids Surf., B* **2011**, *86*, 111−118.
(28) Lee, H.; Scherer, N. F.; Messersmith, P. B. *Proc. Natl. Acad. Sci. U.S.A.* **2006**, *103*, 12999−13003.
(29) Bradford, M. M. *Anal. Biochem.* **1976**, *72*, 248−254.
(30) etinus, Akku; Nursevin ztop, H. *Enzyme Microb. Technol.* **2003**, *32*, 889−894.
(31) Lee, B. P.; Dalsin, J. L.; Messersmith, P. B. *Biomacromolecules* **2002**, *3*, 1038−1047.
(32) Lee, Y.; Chung, H. J.; Yeo, S.; Ahn, C. H.; Lee, H.; Messersmith, P. B.; Park, T. G. *Soft Matter* **2010**, *6*, 977−983.
(33) Sever, M.; Wilker, J. *Dalton Trans.* **2006**, *2006*, 813−822.
(34) Butler, A. *Science* **1998**, *281*, 207.
(35) Fakhrullin, R. F.; Minullina, R. T. *Langmuir* **2009**, *25*, 6617−6621.
(36) Kurth, D. G. *Ann. N.Y. Acad. Sci.* **2002**, *960*, 29−38.
(37) Lee, H.; Rho, J.; Messersmith, P. B. *Adv. Mater.* **2009**, *21*, 431−434.
(38) Cosulich, M.; Russo, S.; Pasquale, S.; Mariani, A. *Polymer* **2000**, *41*, 4951−4956.
(39) Alptekin, Ö.; Tü1kel, S. S.; YIldIrIm, D.; Alagöz, D. *J. Mol. Catal. B: Enzym.* **2010**, *64*, 177−183.